Clustering of rRNA operons in *E. coli* is disrupted by σ^H

Khang Ho and Rasika M. Harshey*

Department of Molecular Biosciences and

LaMontagne Center for Infectious Diseases,

The University of Texas at Austin,

Austin, Texas, 78712, USA

* Corresponding author: rasika@austin.utexas.edu

Abstract

Chromosomal organization in *E. coli* as examined by Hi-C methodology indicates that long-range interactions are sparse. Yet, spatial co-localization or 'clustering' of 6/7 ribosomal RNA (*rrn*) operons distributed over half the 4.6 Mbp genome has been captured by two other methodologies - fluorescence microscopy and Mu transposition. Our current understanding of the mechanism of clustering is limited to mapping essential *cis* elements. To identify *trans* elements, we resorted to perturbing the system by chemical and physical means and observed that heat shock disrupts clustering. Levels of σ^H are known to rise as a cellular response to the shock. We show that elevated expression of σ^H alone is sufficient to disrupt clustering, independent of heat stress. The anti-clustering activity of σ^H does not depend on its transcriptional activity but requires core-RNAP interaction and DNA-binding activities. This activity of σ^H is suppressed by ectopic expression of σ^D suggesting a competition for core-RNAP. A query of the other five known σ factors of *E. coli* found that elevated expression of FecI, the ECF σ factor that controls iron citrate transport, also perturbs clustering and is also suppressed by σ^D. We discuss a possible scenario for how these membrane-associated σ factors participate in clustering of distant *rrn* loci.

Introduction

Bacteria inhabit every available niche on earth, where they are subject to a range of environmental conditions to which they must acclimatize [1]. When conditions are favorable, bacteria quickly synthesize proteins required for uptake and biosynthesis of cellular building blocks that enable virtually every aspect of cell growth [2]. The bulk of cellular transcription during this phase is dedicated to *rrn* operons that synthesize ribosomes. Not only are *rrn* operons highly transcribed, but most bacteria also possess multiple such operons. The multiplicity of *rrn* operons has been correlated with elevated growth rate, genome integrity and acquisition of more diverse biosynthetic pathways [3,4], suggesting that there is an evolutionary advantage to maintaining multiple copies of these operons.

There are seven *rrn* operons in *E. coli* (*rrn*A-G), distributed on both arms (replicores) of the bi-directionally replicating chromosome, and residing in the upper half of each replicore [5] (Fig. 1). FROS (Fluorescent Reporter Operator Sites) experiments using pairwise *parS*-ParB interactions showed that 6/7 *rrn* loci spatially co-localize or cluster, reminiscent of the eukaryotic nucleolus [6]. This cluster was not detected by the more widely used Hi-C methodology, which employs formaldehyde to crosslink chromosomal interactions bridged by proteins [7]. Failure to detect the *rrn* cluster by this method could be due to disruption of the cluster by formaldehyde, or to a distance unfavorable for crosslinking. An alternative crosslinking method that exploits the natural mechanism of phage Mu transposition to link distant DNA sites indeed detected the *rrn* cluster [8]. The Mu method is not widely used as yet, because of the limited host-range of Mu, but has been additionally validated by corroborating the existence of a distinct Ter region on the *E. coli* genome [9], as demonstrated using other techniques [7,10].

The FROS study delineated *cis*-acting elements required for *rrn* clustering by systematically deleting regulatory regions upstream of *rrnD* and monitoring its co-localization with

51 *rrnG*, both located on the same arm of the chromosome but separated by 700 kbp (Fig. 1) [6].
52 The study found that clustering required P1, the stronger of the two promoters driving transcription
53 of *rrnD*, as well as an upstream binding site for the NAP (Nucleoid Associated Protein) Fis, but
54 that neither Fis nor other NAPs known to regulate *rrn* transcription were required, suggesting that
55 transcription of the *rrn* locus was not responsible for clustering. Consistent with this notion,
56 mutation of the conserved -10 region of P1 failed to disrupt clustering, indicating that the formation
57 of an open complex was also dispensable. Taken together, these results indicated that multiple
58 transcribing RNA polymerases expected at these highly transcribed loci are likely not the cause
59 of clustering. The Mu method showed that the NAP HUα influenced cluster formation, likely by
60 affecting chromosome compaction in general [8].

61 To gain more insight into the phenomenon of *rrn* clustering we attempted to perturb the
62 system by subjecting cells to amino acid starvation, as well as to heat, cold and ethanol shock.
63 Of these, heat shock completely disrupted clustering. The heat shock response, part of the more
64 general unfolded protein response [11], is designed to maintain heat-denatured proteins in a
65 properly folded state, a key player in this response being σ^H [12]. σ^H (RpoH) regulates a large
66 number of genes, notably those encoding protein chaperones such as GroEL/GroES [13,14]. We
67 show that it is the rise in σ^H levels and not heat stress *per se*, that disrupts clustering and
68 corroborate this observation using the Mu method. The observed σ^H-promoted de-clustering could
69 be counteracted by simultaneous expression of σ^D (or σ^{70}). A similar but weaker effect on de-
70 clustering was exhibited by FecI, which was also rescued by σ^D. Both σ^H and FecI are associated
71 with the inner membrane. Based on these findings, we propose a model for how clustering of *rrn*
72 operons occurs at the membrane and might be driven by the ability of sigma factor(s) to assemble
73 RNAP onto cognate promoters.

74

75 # Results

76 ## Heat shock disrupts *rrnA-rrnD* clustering

77 Gaal et al. used FROS to examine pair-wise combinations of fifteen of the possible twenty-one
78 pairs of *rrn* operons, using distinct *parS*-ParB partners derived from phage P1 and plasmid pMT1
79 of *Yersinia pestis* (Fig. S1) [6,15]. In this study, we employed the same approach to determine
80 *trans*-acting factors involved in clustering (Fig 2A). For our analysis we chose *rrnA* and *rrnD*,
81 located on two different replicores (Fig. 1), directing ParB-GFP 361bp upstream of *rrnA* and ParB-
82 CFP 282 bp upstream of *rrnD* by inserting their respective *parS* sites at these locations (Fig. 2A);
83 median *rrnA-D* distance was estimated to be 134 nm. These cells were then subjected to various
84 well-studied chemical and physical stresses (Fig. 2B). Serine hydroxamate (SHX) is a serine
85 analog that inhibits $tRNA^{ser}$ aminoacylation, mimicking amino acid starvation and inducing a
86 stringent response with concomitant synthesis of (p)ppGpp [16,17]. Application of this stress failed
87 to produce a notable change (>2-fold) in the median *rrnA-D* distance (214 nm, compared to a
88 significance cutoff at 230 nm; see figure legend for assignment of significance). Cold shock, which
89 elicits changes in membrane fluidity, protein and nucleic acid folding and ribosome assembly [18],
90 also did not significantly perturb clustering (216 nm). Ethanol damages cell wall and membrane
91 integrity, inducing an unfolded protein response in addition [11,19]. This stress increased the *rrnA-*
92 *rrnD* distance to 424 nm. The unfolded protein response can also be produced by heat stress,
93 which produced the most pronounced shift of the median distance relative to control (734 nm)
94 (Fig 2B). Representative images from these experiments are shown in Figure 2C-D. We note that
95 heat stress appears to localize *rrnA*, but not *rrnD*, to the pole, while also reducing the number of
96 *rrnA* loci to 1 (Fig 2D, green arrow). Since ethanol also induces the unfolded protein response,
97 we infer that it is the unfolded protein response that promotes de-clustering of *rrnA* and *rrnD*.

98 Since our laboratory has shown that long-range contacts occur less frequently in an *hupA*
99 (HUα) mutant [8], we also examined a noncoding (nc) RNA known to interact with HU [20]. A

100 single deletion of nc5 showed no difference in the median distance between *rrnA* and *rrnD* (Fig.
101 S2). RpoZ (an RNAP subunit) and NusB (a component of the anti-termination complex that
102 interacts with RNAP), reported to contribute to phase-separation of *E. coli* RNAP [21], were also
103 examined. Deletion of either *rpoZ* or *nusB* elicited a small increase (i.e. above our 2-fold cutoff of
104 230 nm) in the *rrnA-D* distance (254 nm and 304 nm, respectively) (Fig S2), but not as drastic as
105 that of heat stress.

106 In summary, of all the variables tested, heat stress caused the most significant de-
107 clustering of the *rrnA-D* pair, followed by ethanol stress. These two stresses share the common
108 outcome of producing an unfolded protein response.

109

110 **Deregulation of GroEL/S disrupts *rrnA-rrnD* clustering**

111 Since heat shock disrupted the *rrnA-D* pair, we hypothesized that some protein factor(s) bridging
112 the two loci was displaced as a result. To identify bound proteins, we directed dCas9 (a variant of
113 Cas9 capable of binding but not cleavage [22]), to upstream regions of all seven *rrn* loci, similar
114 to the location of *parS* sites (see Table S2), using the appropriate gRNAs. dCas9 was fused to
115 3X-FLAG, so anti-FLAG antibodies were used in pulldown experiments (Fig. 3A). The efficiency
116 of sgRNA targeting was determined by assessing lethality when Cas9 was provided instead of
117 dCas9 (Fig. S3). Overall, in a host expressing Cas9, sgRNAs directed to all *rrn* operons caused
118 a reduction in viability relative to a no-PAM control (Fig. S3). The differences in gRNA efficiency
119 may influence the efficiency of dCas9 pulldowns, but since Cas9 targeting was productive, we
120 concluded that the pulldowns would reflect at least the binding of dCas9 to the rDNA.

121 Mass spectrometry of the proteins identified in pull-downs with the seven *rrn* samples showed
122 a range of significantly enriched proteins across different sgRNAs (z-score> 2.5, computed from
123 three biological replicates for each sgRNA) using the methods described in [23]. Common

124 proteins identified across multiple samples are summarized in Fig. 3B. For sgRNA targeting *rrnA,*
125 *rrnB, rrnC, rrnD, rrnE, rrnG,* and *rrnH*, we found 54, 132, 135, 105, 66, 33 and 107 significantly
126 enriched proteins, respectively (Fig. 3C and Fig. S4). The detailed spectral counts of identified
127 proteins for each sgRNA can be found in Tables S3-S9. No common protein was significantly
128 enriched across all samples, but GroEL was enriched in 4/7 sgRNAs (*rrnC, rrnA, rrnB,* and *rrnD*),
129 suggesting that GroEL could be a possible *trans*-acting factor in clustering.

130 GroEL, in complex with GroES, acts as a chaperone for protein folding [24]. To investigate
131 whether GroEL mediated *rrn* clustering, we generated a chromosomal *groEL* deletion in the *parS*-
132 tagged *rrnA-D* strain (Fig. 3D). Since *groEL* is essential [25], we provided it in *trans* from a plasmid
133 under control of pAraBAD and verified induction (with arabinose) and repression (with glucose)
134 by observing corresponding increases and decreases in colony sizes, respectively (Fig S5).
135 Examination of the degree of *rrnA-rrnD* clustering under these two conditions showed that
136 clustering was disrupted with arabinose addition (Fig. 3, third plot from the left), even though
137 GroEL levels were sufficient for growth as judged by colony size (Fig. S5); the median distance
138 between *rrnA-D* increased to 494 nm. A WT 'control' carrying both *groEL*/*groES* under pAraBAD
139 control increased *rrnA-D* distance to 216 nm (Fig. 2D, second plot from left); this slight increase
140 is not significant based on our 2-fold cut-off, but the data nonetheless suggest that ectopic
141 expression *of groES/EL* affects clustering. Taken together, these results suggest that any
142 perturbation of normal GroES/EL levels destabilize clustering. Since these two genes are co-
143 transcribed [26], we wondered if the imbalance in their relative levels was responsible for cluster
144 disruption. We therefore placed the entire *groES/EL* operon on the plasmid vector in the Δ*groEL*
145 strain, but that did not restore clustering either (Fig. 3D, rightmost plot).

146 To test if expression of *groES/groEL* from their native σ^H-promoter (pGroE) would change the
147 results, we compared *rrnA-D* distance when expression of this operon was controlled by pGroE
148 vs pAra in both WT and Δ*groEL* strains (Fig. 4E). A shift closer to normal in the *rrnA-D* distance

149 as indicated by the 25% quartile of 242 nm for pGroE vs 356 nm for pAra (Fig 3E, compare
150 rightmost two plots), suggests that transcription from the native promoter was better at restoring
151 clustering. σ^H, also known as σ^{32} or RpoH, is the major heat shock sigma factor that transcribes
152 the *groEL/S* operon exclusively [26]. Its levels are kept low through multiple mechanisms,
153 including sequestration at the inner membrane, and direct interaction of GroEL/ES with σ^H [27,28].
154 Could our inability to restore *rrnA-rrnD* clustering in the Δ*groEL/ES* background be attributable to
155 perturbation of σ^H levels? This was tested next.

156

157 **σ^H disrupts *rrnA-rrnD* independent of its transcriptional activity**

158 If perturbation of σ^H was the cause of *rrnA-D* de-clustering, we hypothesized that ectopic
159 expression of σ^H alone should give similar results. We therefore placed *rpoH* under an inducible
160 Tet promoter (pTc). Consistent with our expectations, *rpoH* induction increased the median
161 distance between *rrnA-D* to 566 nm (Fig 4A, third plot from left). However, the same result was
162 seen even in the absence of *rpoH* induction (Fig. 4A, second plot from left). To verify that *rpoH*
163 was being expressed from the plasmid, we constructed a *lacZ* reporter driven from p*htpG*, a weak
164 σ^H-responsive promoter [29], and assessed *lacZ* expression upon induction of *rpoH* from pTc (Fig
165 4B). A small but significant increase in β-galactosidase activity was observed after an hour of
166 induction, the same time frame employed for microscopy (Fig. 4A), indicating that *rpoH* was
167 expressed from the Tet promoter. We conclude that even a small increase in σ^H levels promotes
168 de-clustering of *rrnA-rrnD*.

169 *E. coli* possesses seven experimentally confirmed sigma factors, of which the vegetative
170 σ^D (RpoD or σ^{70}) is the most abundant [30]. Since the amount of RNAP is thought to be relatively
171 constant across most growth conditions, competition among the sigma factors for this core RNAP
172 has been proposed to be the mechanism for gene regulation [30,31]. To test if competition

173 between σ^H with σ^D for binding RNAP could be responsible for destabilizing clustering, we inserted
174 *rpoD* downstream of TetR on the same plasmid, which is driven by the constitutive promoter
175 divergent from pTc (pTetR). Expression of *rpoD* decreased the median distance between *rrnA-D*
176 to 213 nm compared to 566 nm with the *rpoH* vector alone (Fig 4A, compare fourth plot to second
177 plot from the left), supporting the notion that competition between σ^D and σ^H for core RNAP likely
178 suppressed the de-clustering activity of σ^H.

179 To test this notion further, we examined the following previously characterized mutants of
180 *rpoH,* reported to have decreased or increased transcription activities: L245P is defective for
181 interaction with RNAP [32], E265A is defective for promoter binding at the -35 region [32], and
182 I54N has increased stability [28,29] . Our expectation was that the L245P and E265A would lose
183 their de-clustering activity, while I54N mutant would not. This expectation was borne out for the
184 L245P and E265A variants (303 nm and 216 nm, respectively), but not for I54N (284 nm) i.e. all
185 three variants were defective in destabilizing the *rrn* cluster, compared to WT RpoH (566 nm) (Fig
186 4C). We note that in contrast to cells expressing the first two variants, those expressing I54N are
187 elongated (Fig S6). I54N has been shown to exhibit elevated transcriptional activity due to its
188 inability to localize to the membrane like WT σ^H [27,29], which likely perturbs normal cell
189 physiology. The expected transcriptional activity of all the σ^H mutants was confirmed using the
190 *lacZ* reporter as before (Fig. 4D). We conclude that σ^H -mediated de-clustering is independent of
191 its transcriptional activity.

192

193 **σ^H does not disrupt all *rrn* pairs**

194 Our experiments thus far queried the co-localization of the *rrnA-rrnD* pair as representative of all
195 the *rrn* loci found in the cluster [6]. To test if heat shock and σ^H were equivalent in their disruptive
196 ability, we decided to query other pairs, including every co-localizing *rrn* operon at least once, with
197 *rrnC* as the non-clustering control. Heat shock disrupted clustering of all non-C *rrn* operons tested,

198 the median distance increasing 1.5 - 2.5 fold (from 80-120 nm to 450-700 nm) (Fig 5A; summary
199 of the results diagrammed in Figure 5B). *rrnC* is reported to not be part of the cluster [6,8], yet its
200 distance from *rrnG* remained curiously unperturbed by heat, staying at ~400nm median,
201 suggesting perhaps a specificity to clustering that supersedes the global unfolding effect of heat
202 stress.

203 The effect of σ^H on the *rrn* pairs tested was non-uniform (Fig. 5C). Specifically, we
204 observed that two pairs that shared *rrnH* appeared to be resistant to disruption by σ^H (Fig 5C).
205 Thus, contacts between all the *rrn* loci in the cluster are not uniform, suggesting that there is likely
206 a sub-organization within this structure.

207 To determine if σ^H played a unique role in affecting cluster stability, we ectopically
208 expressed the other five sigma factors: RpoE (σ^{24}), RpoF (σ^{28}), RpoN (σ^{54}), RpoS (σ^{38}) and FecI
209 (σ^{19}), under the same promoter as the *rpoH*-expressing vector, maintaining the same RBS
210 (ribosome binding site). Of these, FecI produced a smaller destabilizing effect (84 nm vs 234 nm
211 for RpoH) (Fig. 5D). To test if σ^D would restore clustering to the FecI-expressing strain like it did
212 when co-expressed with σ^H (Fig. 4A), we co-expressed *rpoD* with *fecI*; clustering was completely
213 restored wild type levels (Fig. 5D, compare last two plots). We note that the shared properties of
214 RpoH and FecI are that they are both normally sequestered at the inner membrane, suggesting
215 perhaps that *rrn* clustering may have a membrane component.

216

217 **σ^H disrupts the *rrn* cluster as tracked by the Mu method**

218 Phage Mu transposition requires direct contact between Mu and its transposition target and
219 displays virtually no sequence specificity in its target choice [33]. Higher or lower frequencies of
220 transposition are therefore interpreted to reflect higher or lower rates of physical contact between
221 the interacting chromosomal regions, analogous to the contact frequencies inferred from
222 normalized Hi-C data [34]. Contacts made by Mu when located next to *rrnD* showed significantly

223 positive interaction between *rrnD* and chromosomal regions containing the *rrnA, B, E, G, and H*
224 (but not *rrnC*), suggesting physical proximity of these regions, as also seen by FROS [6].

225 Since we did not examine the effect of σ^H on all possible combinations of *rrn* loci with
226 FROS (Fig. 5), we used the Mu method to examine transposition patterns of Mu located near *rrnD*
227 in the presence of ectopically expressed RpoH. The pattern of Mu transposition from the *rrnD*-
228 proximal locus in WT cells was consistent with the earlier report, where Mu could access every
229 region of the chromosome irrespective of its starting location (Fig 6A). In the presence of the
230 vector encoding RpoH, even without induction of RpoH expression, the transposition landscape
231 was altered, with more Mu insertions now occurring proximal to the starting Mu in Bin 72 (Fig 6B).
232 This increase in local versus distal contacts is not exacerbated with *rpoH* induction (Fig 6C),
233 similar to microscopy data (Fig. 4A). Transposition frequencies across different conditions are
234 summarized in Fig 6D. Even though Mu insertion frequency at its starting bin is the highest across
235 all conditions, in the presence of *rpoH* overexpression, a global decrease is seen in the non-
236 starting bins (RpoH and +RpoH column compared to None column), indicating that *rpoH*
237 overexpression disrupts long-range contacts.

238 We next examined specifically the bins containing *rrn* operons to assess the effect of RpoH
239 on Mu transposition. We observed that contact between *rrnD* and a majority of the *rrn* loci
240 decreased, with the notable exception of those with *rrnC* and *rrnH*, which remain unchanged (Fig.
241 6E). The *rrnC* result is consistent with earlier reports [6,8], and the *rrnH* result is consistent with
242 data in Figure 5C, where RpoH promoted de-clustering of all *rrn* examined, with the exception of
243 *rrnH*. Overall, Mu transposition data support the hypothesis that σ^H promotes de-clustering of *rrn*
244 operons.

245

246 **Discussion**

247 This study demonstrates that the *E. coli* 'nucleolus' where 6/7 *rrn* operons are reported to co-
248 localize, can be perturbed by the cellular heat shock response as demonstrated by both FROS
249 and Mu transposition. This perturbation is not due to heat stress per se, but rather due to elevation
250 of RpoH or σ^H levels known to occur during the response. We discuss below what this and other
251 data may suggest about the mechanism of co-localization of the *rrn* operons.

252

253 **Ability to disrupt its organization validates the existence of the *E. coli* 'nucleolus'**

254 In eukaryotic cells, the nucleolus is the primary site of ribosome biogenesis [35]. It is a large
255 structure, where hundreds to thousands (depending on the organism) [36], a device thought to
256 have evolved to maximize translation efficiency [35]. By contrast, *E. coli* has only seven operons
257 encoding ribosomal DNA (*rrn* operons) [37] (Fig. 1). That 6/7 of these operons come together is
258 some as-yet unknown fashion was first reported by Gaal et al. using FROS methodology, who
259 called this organization a 'bacterial nucleolus' and showed that its presence was independent of
260 growth media and of cell doubling times [6]. A completely different Mu methodology detected the
261 proximity of the same 6/7 *rrn* operons [8], providing strong support for this observation.

262 Gaal et al. found that the only *cis* elements required for formation of the *E. coli* nucleolus
263 were the P1 promoter and an UP element that contained FIS binding sites in one of the interacting
264 *rrn* pairs tested (Fig. 1). However, neither Fis nor active *rrn* transcription was required, as gleaned
265 from recalcitrance of the *rrn* cluster to disruption by addition of rifampicin, which stops RNA chain
266 elongation [38], as well to mutation of a -10 region in the P2 promoter that prevents open complex
267 formation that signals initiation of transcription. These properties of the *E. coli* nucleolus are in
268 contrast to the requirement for Pol I function and rRNA transcription to maintain nucleolar
269 structure and integrity in eukaryotic cells [39]. We will therefore simply call this co-localization an
270 *rrn* cluster.

271 To learn more about the nature of the *rrn* cluster, we attempted to perturb it by exposing
272 cells to several environmental stressors (Fig. 2B). Of these, heat and ethanol shock had the
273 largest effect. These two stressors share a common 'unfolded protein' response [11]. The
274 important take-away from this experiment is that by perturbing the cluster, we had not only
275 validated its existence but found a handle to probe its nature.

276

277 The heat shock response, GroEL/GroES and σ^H all destabilize the *rrn* cluster: σ^D 278 counteracts the action of σ^H

279 Adaptation to heat shock is a universal biological phenomenon [11]. Heat denatures proteins, so
280 organisms adapt by synthesizing protein-folding chaperones. *E. coli* encodes several chaperones
281 including GroEL/GroES and employs σ^H to transcribe hundreds of genes that enable bacterial
282 survival [13,14]. The ability of heat shock to disrupt the *rrn* cluster suggested to us that proteins
283 must participate in holding the structure together at some level. We therefore directed FLAG-
284 tagged dCas9 immediately upstream of each of the 7 *rrn* loci, followed by pull-down with FLAG
285 antibodies and mass spectroscopy. No common protein was significantly enriched across all
286 samples, but GroEL was enriched in 4/7 sgRNAs (*rrnC, rrnA, rrnB,* and *rrnD*), suggesting that
287 GroEL could be a possible *trans*-acting factor in clustering (Fig. 3A-C; Fig. S4). (Although *rrnC* is
288 not part of the cluster, it is close to the origin of replication *ori*, and it is conceivable that unrelated
289 events at *ori* block its incorporation into the cluster).

290 To query the participation of GroEL directly, we attempted to delete the chromosomal copy
291 of this essential gene while providing it ectopically from either a regulated promoter or its native
292 promoter. Both manipulations disrupted the *rrn* cluster, although expression from its native
293 promoter was slightly less disruptive (Fig. 3E). The *groEL/S* operon is transcribed exclusively by
294 the major heat shock sigma factor σ^H, whose levels are kept low through multiple mechanisms,

295 including sequestration at the inner membrane where it is degraded by protease FtsH, as well as
296 direct interaction with GroEL/ES [27,28]. To test if our manipulations of GroEL were perturbing σ^H
297 levels, we provided RpoH ectopically from a regulatable promoter. Even in the absence of
298 induction, leaky expression of RpoH was sufficient to disrupt the *rrn* cluster (Fig. 4A).

299 Why should an apparently slight rise in σ^H levels have such a profound effect on stability
300 of the cluster? Given that the P1 promoter and its UP elements participate in maintaining the
301 cluster, we imagined a scenario where RNAP bound to the housekeeping σ^D, known to transcribe
302 the *rrn* operons [5], was stationed there and that σ^H might be competing with it for binding RNAP,
303 displacing it and disrupting the structure. We tested this conjecture by inserting *rpoD* along with
304 *rpoH* on the ectopic vector. This resulted in significant cluster rescue compared to *rpoH* alone (Fig
305 4A), supporting our conjecture.

306

307 Sigma factors that disrupt the *rrn* cluster associate with the membrane, suggesting 308 a model for *rrn* clustering

309 RNAP levels in *E. coli* are constant, so competition among the sigma factors for the core RNAP
310 has been proposed to be the mechanism for gene regulation [31]. This competition model predicts
311 that mutants of σ^H that are defective for either RNAP-core or DNA-binding should not disrupt the
312 cluster. We tested this by querying two RpoH mutants, one defective for interaction with RNAP
313 and the other defective for promoter binding at the -35 region. Both mutants were significantly
314 deficient in the de-clustering activity of WT RpoH (Fig. 4C), in keeping with the competition model.

315 σ^H levels are regulated by at least three mechanisms: control through GroEL/GroES,
316 DnaJ/K/GrpE, control of translation efficiency at the mRNA level, and the degradation of σ^H by
317 FtsH, an integral-membrane protease. A third RpoH mutant we tested for its de-clustering activity
318 was I54N, shown to escape FtsH-mediated proteolysis through the inability of the SRP (Signal

319 Recognition Particle)-ffh complex to recognize a patch of amino acids between domain 1 and
320 domain 2 of RpoH, which would result in its being trafficked to the inner-membrane for degradation
321 by FtsH. Our expectation was that this mutant would behave like WT RpoH. Despite its high
322 transcription activity (Fig. 4D), however, the effect of the I54N mutant did not align with our
323 expectations (Fig. 4C), showing at the very least that high levels of transcription directed by σ^H
324 are not the cause of de-clustering, and that none of the members of the σ^H regulon are involved
325 in de-clustering. So why did the I54N mutant not behave like WT RpoH? Unlike the WT protein,
326 I54N mutant is unable to localize to the membrane, suggesting that access to the membrane is
327 important for the de-clustering effect of RpoH, ergo, the *rrn* cluster might be anchored in the
328 membrane.

329 When we tested the cluster-disrupting ability of five other sigma factors - RpoE (σ^{24}), RpoF
330 (σ^{28}), RpoN (σ^{54}), RpoS (σ^{38}) and FecI (σ^{19}) - we found that that FecI, an extracytoplasmic-
331 function (ECF) σ factor, also disrupted clustering, although not as severely as σ^H (Fig. 5D). FecI,
332 along with FecA and FecR, is responsible for the transcription of the ferric citrate transport system,
333 consisting of *fecABCDE* transport genes [40]. FecA is an outer membrane protein that transports
334 $(Fe^{3+}\text{-citrate})_2$ across the outer membrane. Upon binding of $(Fe^{3+}\text{-citrate})_2$ to FecA, the signal is
335 then transduced through the periplasmic face of FecR, an inner membrane protein, to its
336 cytoplasmic face [41,42]. This conformational change of FecR activates the transcriptional activity
337 of FecI in the cytoplasm and promotes transcription of *fecABCDE* [43]. The dependence of FecI
338 on FecR, which is localized to the inner-membrane, for efficient transcription by RNAP-FecI of the
339 *fec* operons, also lends support to a model where the site of *rrn* clustering is the inner membrane.

340 In contrast, overexpression of σ^E, which is also an ECF, failed to disrupt clustering [44,45].
341 The mode of regulation of σ^E is based on the repression of σ^E by the inner membrane anti-sigma
342 factor RseA, which is sandwiched between domain 2 and domain 4 of σ^E, thereby inhibiting the
343 interaction of RNAP core and σ^E [46,47]. Upon membrane stress, such as ethanol or heat, DegS

344 is activated by the presence of unfolded outer-membrane proteins, and, in concert with RseP,
345 degrades RseA, releasing σ^E to promote transcription of downstream genes [48,49]. The negative
346 regulation by RseA may explain why overexpression of σ^E alone is unable to disrupt clustering. In
347 other words, for efficient disruption of the *rrn* cluster, σ^D-independent transcription needs to occur
348 at the inner membrane.

349 Taken together, we propose that clustering of *rrn* is mediated by σ^D at the membrane either
350 through σ^D directly or through other unknown factor(s) (Fig. 7). σ^D has indeed been observed at
351 the membrane [28]. Given that high levels of transcription are not required, but the *cis*-acting
352 elements responsible for high transcriptional activity of *rrn* are, and that some σ factors can disrupt
353 clustering implicating σ^D as the clustering factor, we propose that the assembly of RNAP
354 holoenzyme and UP element features of P1 drives *rrn* clustering. Upon heat stress or elevated
355 σ^H levels, RNAP complexes bound to σ^D are displaced through competition with σ^H, and to a
356 lesser extent FecI, for RNAP core, resulting in de-clustering of *rrn* operons. The order of RNAP
357 assembly has been shown to be $\alpha_2 \rightarrow \beta \rightarrow \beta' \rightarrow \sigma$ [50] or $\alpha_2 \rightarrow \beta \rightarrow \beta' \omega \rightarrow \sigma$ [51]. The requirement for
358 the P1 promoter may reflect the high affinity of α for the UP element present upstream of the -35
359 element [52]. The dimerization of the α subunit could drive the bridging interaction between the
360 disparate *rrn* operons. However, this interaction by itself is unable to explain *rrn* clustering as
361 demonstrated by de-clustering effect of σ^H and FecI, since σ factor binding and unwinding of the
362 DNA duplex is the last step of RNAP assembly. Therefore, we propose that two elements are
363 responsible for *rrn* clustering: (1) the high affinity of α for the UP element, and (2) DNA binding
364 driven by σ^D. The affinity of α for the *rrn* UP element would explain why *rrn* clustering does not
365 extend to other non-*rrn* loci. The specificity of σ^D for the *rrn* promoter would explain the de-
366 clustering activity of σ^H and FecI. We note that σ^H did not affect the position of two pairs that
367 shared *rrnH* (Fig 5C), suggesting a likely a sub-organization within this structure. Finally, why did
368 we recover GroEL at 4/7 rDNA loci (Fig. 3A-C and Fig. S4)? One possibility is that GroEL is meant

369 to clear σ^H from the cluster [27]. Alternatively, since GroEL has been shown to restore
370 transcription of heat-treated RNAP *in vitro* [53], it could either be interacting non-specifically with
371 some component of RNAP or ensuring that the proteins at the cluster do not aggregate.

372

373 **Relationship of the *rrn* cluster to RNAP condensates**

374 RNAP has been reported to form distinct clusters on the *E. coli* nucleoid [54,55]. Since the bulk
375 of cellular transcription is dedicated to rRNA transcription and since RNAP clusters form in fast-
376 growth conditions, it was proposed that these clusters represent high concentrations of RNAP on
377 *rrn* operons [56]. Subsequent work showed that RNAP clusters colocalize with nascent rRNA, but
378 that their spatial arrangement was not dependent on rRNA synthesis activity and was likely
379 organized by the underlying nucleoid [57]. RNAP clusters have been shown to be biomolecular
380 condensates capable of phase separation, involving known factors associated with RNAP (i.e. ω
381 subunit of RNAP, and NusB) [21].

382 The properties of the *rrn* cluster are on the one hand reminiscent of RNAP condensates
383 in that high level of transcription of rRNA is not required for their organization, but, on the other
384 hand, are different in that the cluster is immune to transcription inhibitors while the condensates
385 are not [57]. For example, neither treatment of transcriptional inhibitor Rifampicin (Rif) nor SHX,
386 which inhibits rRNA transcription through the formation of (p)ppGpp, disrupts the cluster [6]. The
387 cluster is unlikely to serve as a precursor for formation of RNAP condensates since these form in
388 a strain where only one *rrn* operon is present [48]. Antitermination factors such as NusB and ω
389 subunit of RNAP have been shown to contribute to formation of RNAP condensates [23].
390 However, we showed in this study that neither Δ*nusB* nor Δ*rpoZ* strains significantly impact the
391 cluster (Fig. S2). We interpret these results to mean that RNAP condensates represent a feature

392 of highly active transcription that the *rrn* cluster contributes to by making rDNA readily available
393 through spatial localization.

394

395 Acknowledgments

396 We thank Rick Gourse for providing pFHC2973, and *parS*-labelled *rrn* strains, Ian Molineux for
397 providing the parent strain that supports replication of R6K origin plasmids, Kamyab Javanmardi
398 for providing Golden Gate vector for gRNA insertion, Rachael Cox and Edward Marcotte for script
399 and computing power used in mass spectrometry analysis, Lydia Freddolino for suggesting use
400 non-Mu reads to correct for replication effects, and Brady Wilkins for assistance with Southern
401 Blot. This work was supported by NIH grant GM118085.

402

403 Materials and Methods

404 **Media, Strains, Phages and Plasmids**. Unless conditions are specified, all strains are grown in
405 LB at 30°C with shaking. When appropriate, antibiotics were at the following concentrations:
406 Ampicillin (Amp) at 100μg/mL, Kanamycin (Kan) at 25μg/mL, Chloramphenicol (Cam) at 20μg/mL.
407 Anhydrotetracycline (aTc) was used for induction of Tet promoter at 50ng/mL. Isopropyl-β-D-
408 Galactoside (IPTG) was used to induce the *lac* promoter at 1mM. o-nitrophenyl-β-D-Galactoside
409 (ONPG) was purchased from Sigma. Competent cells for transformation were prepared by
410 washing a growing culture of O.D. 0.4-0.5 in cold 10% glycerol 3 times. The pellet was
411 resuspended in 1:100 of the original volume in 10% glycerol. Electroporation was performed in *E.*
412 *coli* Pulser (Biorad) with 1mm Electroporation cuvette Plus (Fisher) at 1.8V. Cells were recovered
413 in SOC (LB supplemented with 10mM $MgCl_2$, 10mM $MgSO_4$, and 0.2% Glucose) for 1.5 hours at
414 30°C with shaking prior to plating on the appropriate selection. Mu phage was stored in Mu Buffer

415 (50mM Tris-HCl pH 8.0, 100mM NaCl, 5mM $CaCl_2$, 5mM $MgCl_2$, and 0.1% gelatin). Strains and
416 Phages employed in this study are listed in Table S1. Primers, purchased from Integrated DNA
417 Technology (IDT), used in this study are listed in Table S2.

418 **General Molecular Techniques**. Routine PCR were performed with Taq DNA Polymerase
419 (NEB), according to manufacturer's instructions. PCR fragments for cloning were generated with
420 Phusion DNA Polymerase (NEB) according to manufacturer's instructions. Gibson Master Mix
421 was made according to Gibson *et al* [58]. Gibson assembly was performed at 50°C for at least 2
422 hours. Golden Gate Assembly was performed with Esp3I (NEB), T7 DNA Ligase (NEB), T4 DNA
423 Ligase Buffer (NEB). Primers used to generate the gRNA were used at 10nM each. 100ng of the
424 destination vector was used. The program for Golden Gate Assembly was 3 minutes at 37°C, 2
425 minutes at 16°C for 35 cycles, followed by 1 cycle of 10 minutes incubation at 37°C. T4 DNA
426 Ligase, T4 PNK, and T4 DNA Ligase Buffer were purchased from NEB.

427 **Plasmid Construction**. Plasmids were constructed using Gibson assembly. Typically, 250μL of
428 the backbone was assembled with a molar equivalent of insert in a 20μL reaction. The resulting
429 product was purified with PCR clean-up kit (Qiagen) according to the manufacturer's instructions.
430 2μL of the 20μL eluted product was used for transformation. Colonies were screen by PCR with
431 primers spanning the junction between the backbone and the insert. Positive clones were restruck
432 and checked once more using the same primer pairs. The PCR product was sequenced to confirm
433 the identity of the sequence at either the UT Core Sequencing Facilities or Eton Biosciences. For
434 generating single point mutants, primers carrying the desired mutation were used to amplify the
435 plasmid of interest. The resulting PCR product was gel-extracted with Qiagen Gel Extraction Kit.
436 The product was then self-ligated overnight with T4 DNA Ligase and T4 DNA PNK in T4 Ligase
437 Buffer. The ligated product was then purified and 2μL of the 20μL eluted product was used for
438 transformation. Positive clones carrying the desired mutation were identified by PCR of the target

439 sequence followed by sequencing. The positive clones were then restruck once again and verified
440 with PCR and sequencing.

441 **Strain Construction.** For insertion of *parS* sequences, the procedure was essential was
442 described in [59] with the exception being the template plasmid (pKH3 or pKH4) carrying the
443 appropriate *parS* linked to antibiotic resistance cassette. Briefly, 0.5mL of an overnight culture of
444 MG1655 carrying pKD46 was pelleted, washed twice in 1mL of PBS, and diluted 1:100 in fresh
445 LB supplemented with 0.2% arabinose. The culture was grown to an O.D. of approximately 0.4.
446 The cells were made electrocompetent. Cells were then transformed with the appropriate PCR
447 product and let recover in SOC for 3 hours at 30°C. The outgrowth was then plated on the
448 appropriate selection and incubated at 37°C overnight. Positive clones were identified by PCR
449 with primers amplifying the junction of expected insertion. Positive clones were struck out on the
450 appropriate selection plate at 37°C and reconfirmed with PCR followed by sequencing. To remove
451 the antibiotic-encoding cassette for subsequent insertion of additional *parS*, pCP20 was
452 transformed into the desired host strain. Clones carrying pCP20 were then struck out on LB plate
453 without selection and incubated at 42°C overnight. Colonies were then checked for the loss of
454 both pCP20 and the antibiotics cassette by streaking on the appropriate selection.

455 **Fluorescent Microscopy and Post-Processing.** Overnight cultures used for fluorescent
456 microscopy were grown overnight in EZ-Rich media (Teknova) from single colony and diluted
457 1:100 in fresh EZ-Rich media supplemented with IPTG for induction of ParB-fluorescent fusions
458 from pFHC2973. The subculture grew until an O.D. of 0.4. 1mL of the culture was then pelleted
459 by centrifugation and resuspended in 100μL of PBS. 6uL of the suspension was then spotted onto
460 agarose pad (1%) and let dry. The sample was then observed under Olympus-XM10 camera
461 100x objective with oil immersion. Most images were taken at an exposure of ~100ms for GFP
462 filter, and ~400ms for CFP filter, however, some samples required a longer exposure time to
463 obtain acceptable signal for downstream processing; the upper limit of exposure was 3s. Cellular

464 stressors were applied 20 minutes prior to imaging, after which they were prepared and imaged
465 as described above. For heat stress, the cells were transferred to a 42°C water bath. SHX was
466 added to a concentration of 50μM. Cold stress was 4°C water bath. Ethanol stress was induced
467 by adding ethanol to 0.5%. For image-processing, the background was subtracted from the
468 image, and foci were detected with ImageJ using the detect maxima function. The coordinates of
469 the foci were exported and the Cartesian distance between a GFP focus, and its closest CFP
470 focus was determined with custom Python script. The distance was computed by scaling the
471 distance in pixel to nm with 1 pixel = 62nm. Due to the large number of foci observed, even
472 datasets that produced small differences in the median distance would be statistically significant.
473 We therefore arbitrarily determined that a 2-fold change in median distance is significant.

474 **Pulldown of dCas9 and Proteomics**. Three independent overnight cultures of MG1655 carrying
475 pKH5 and the corresponding gRNA were pelleted and washed as described above. The pellet
476 was diluted 1:100 into 100mL fresh LB supplemented with selection and 0.2% arabinose and aTc.
477 The cultures were grown to an O.D. of 0.6 and pelleted and washed 3 times in 1mL of PBS. The
478 subsequent pulldown procedure was carried out as described by FLAG Immunoprecipitation kit
479 (Rockland). Every step of the pulldown was conducted at 4°C. Briefly, the pellet was resuspended
480 in 5mL of lysis buffer and sonicated (Brason tip, 40% intensity) for 10 minutes (10s on, 10s off
481 cycle). The lysate was clarified by centrifugation at 4°C. Agarose-αFLAG Ab was washed twice
482 in PBS and once in elution buffer. The washed Agarose-αFLAG Ab was incubated with the lysate
483 overnight. After incubation, the beads were collected and washed 3 times with PBS. The bound
484 proteins were eluted with elution buffer. The proteins were quantified by Mass Spectrometry at
485 the UT Proteomics core. Samples were digested with trypsin, desalted and run on Dionex LC
486 (liquid chromomatography) and Orbitrap Fusion 2 (mass spec machine) for 60 minutes. Raw data
487 were analyzed with PD2.2 and Scaffold 5 software. Downstream analysis was performed as

488 described in [23] with lacZ gRNA pulldown as the negative control. Significantly enriched hits were
489 ranked based on a z-score cut-off of 2.5.

490 **Miller Assay**. 0.5mL of three overnight cultures of desired strain carrying the appropriate plasmid
491 was pelleted and washed in 1mL of PBS twice. The pellet was then resuspended in 0.5mL of PBS
492 and diluted 1:100 in LB. The cultures were grown to an O.D. of 0.4 and aTc was added. At
493 indicated time points, 20μL of the culture was withdrawn, its O.D. 600 recorded and added to
494 80μL of permeabilization buffer (100mM $NaHPO_4$, 20mM KCl, 2mM $MgSO_4$, 0.8mg/mL CTAB,
495 0.4mg/mL sodium deoxycholate, 5.4μL/mL β-mercaptoethanol). After the final time point, 600μL
496 of substrate solution (60mM Na_2HPO_4, 40mM NaH_2PO_4, 1mg/mL ONPG, 2.7μL/mL β-
497 mercaptoethanol) was added to each sample. The samples were incubated at 30°C for 60
498 minutes before 600μL of 1M Na_2CO_3 was added to stop the reaction. O.D. 420 was recorded.
499 Miller units were calculated as follows:

500 $$Miller\ Units = 1000 \times \frac{Absorbance_{420nm}}{60 \times Absorbance_{600nm} \times 0.02}$$

501 **Mu Phage Preparation.** When required, lysogen of the indicated prophage was grown overnight,
502 diluted 1:100 in fresh LB and grown until an O.D. of 0.5. After which, the culture was shifted to a
503 42°C waterbath and incubated until lysis is complete. The lysate was clarified by centrifugation at
504 6000g for 20 minutes. The supernatant was transferred to a clean flask and NaCl was added to
505 a final concentration of 0.5M followed by the addition of Polyethylene glycerol 8000 to a final
506 concentration of 10% w/v. The mixture was incubated overnight at 4°C. The pellet was then
507 collected by centrifugation at 8000g for 20 minutes. The pellet was then resuspended in 1:100 of
508 the original volume in Mu Buffer. Chloroform was added to the mixture and shaken. The phases
509 were separated by centrifugation at 4000g for 10 mins at 4°C. The aqueous phase was collected
510 (top layer) and titered prior to use.

511 **Generation of mlaF::Mu and single-transposition experiments**. Selection for Mu insertion at
512 *mlaF* (bin72 as described in [8]) was performed by first introducing *sacB* at *mlaF* followed by
513 infection Mu carrying a Cam marker. Briefly, *attP* was introduced into *mlaF* by λred recombination,
514 and the Kan marker was removed. KH2 was then introduced into this strain, induced for
515 expression of λ Int with arabinose followed by transformation of KH22. Clones positive for
516 integration of the *sacB-kanR* cassette was verified by PCR spanning the expected junction
517 between the cassette and *mlaF*. This strain was then infected with Mu::Cam at an MOI of 5, and
518 survivors that were resistant to sucrose and Cam were selected for. Three colonies were picked
519 and insertion locations for each were confirmed with PCR. Southern Blot was performed to
520 confirm that only one Mu inserted. Of 3 clones picked, one was confirmed to be a mono-lysogen.
521 This strain was designated KH10. Single hop experiment performed with KH10 was performed
522 as described in [8] with modifications for plasmid expression of *rpoH*. For induction of *rpoH* in
523 KH10, overnight cultures were selected for Tet and subsequently grown in LB absent for Tet. 1
524 hour prior to temperature shift for induction of Mu transposition, aTc was added. Genomic DNA
525 was extracted with Wizards Genomic DNA Kit, and sequencing was performed by Novogene on
526 NovaSeq PE150 platform. Partitioning of the genome into 100 bins was as described previously
527 [8]. Data was processed using custom script described in [8] without LASSO regression. Instead,
528 the number of insertions per bin was first corrected for total number of read counts, followed by
529 correcting for replication effect by normalizing to the total number of *E. coli* reads mapped to that
530 bin The average of three biological replicates and standard error was used to plot the data for
531 normalized transposition frequency.

532

533 # References

534 1. Gonzalez JM, Aranda B. Microbial Growth under Limiting Conditions-Future Perspectives.
535 Microorganisms. 2023;11. doi:10.3390/microorganisms11071641

536 2. Bremer H, Dennis PP. Modulation of Chemical Composition and Other Parameters of the Cell at
537 Different Exponential Growth Rates. EcoSal Plus. 2008;3. doi:10.1128/ecosal.5.2.3

538 3. Klappenbach JA, Dunbar JM, Schmidt TM. rRNA operon copy number reflects ecological
539 strategies of bacteria. Appl Environ Microbiol. 2000;66: 1328–1333. doi:10.1128/AEM.66.4.1328-
540 1333.2000

541 4. Fleurier S, Dapa T, Tenaillon O, Condon C, Matic I. rRNA operon multiplicity as a bacterial genome
542 stability insurance policy. Nucleic Acids Res. 2022; 1–20. doi:10.1093/nar/gkac332

543 5. Condon C, Squires C, Squires CL. Control of rRNA transcription in Escherichia coli. Microbiol Rev.
544 1995;59: 623–645. doi:10.1128/mr.59.4.623-645.1995

545 6. Gaal T, Bratton BP, Sanchez-Vazquez P, Sliwicki A, Sliwicki K, Vegel A, et al. Colocalization of
546 distant chromosomal loci in space in e. Coli: A bacterial nucleolus. Genes Dev. 2016;30: 2272–
547 2285. doi:10.1101/gad.290312.116

548 7. Lioy VS, Cournac A, Marbouty M, Duigou S, Mozziconacci J, Espéli O, et al. Multiscale Structuring
549 of the E. coli Chromosome by Nucleoid-Associated and Condensin Proteins. Cell. 2018;172: 771-
550 783.e18. doi:10.1016/j.cell.2017.12.027

551 8. Walker DM, Freddolino PL, Harshey RM. A Well-Mixed E. coli Genome: Widespread Contacts
552 Revealed by Tracking Mu Transposition. Cell. 2020;180: 703-716.e18.
553 doi:10.1016/j.cell.2020.01.031

554 9. Walker DM, Harshey RM. Deep sequencing reveals new roles for MuB in transposition immunity
555 and target-capture, and redefines the insular Ter region of E. coli. Mob DNA. 2020;11: 26.
556 doi:10.1186/s13100-020-00217-9

557 10. Mercier R, Petit MA, Schbath S, Robin S, El Karoui M, Boccard F, et al. The MatP/matS Site-
558 Specific System Organizes the Terminus Region of the E. coli Chromosome into a Macrodomain.
559 Cell. 2008;135: 475–485. doi:10.1016/j.cell.2008.08.031

560 11. Celli J, Tsolis RM. Bacteria, the endoplasmic reticulum and the unfolded protein response: friends
561 or foes? Nat Rev Microbiol. 2015;13: 71–82. doi:10.1038/nrmicro3393

562 12. Grossman AD, Erickson JW, Gross CA. The htpR gene product of E. coli is a sigma factor for heat-
563 shock promoters. Cell. 1984;38: 383–390. doi:10.1016/0092-8674(84)90493-8

564 13. Nonaka G, Blankschien M, Herman C, Gross CA, Rhodius VA. Regulon and promoter analysis of
565 the E. coli heat-shock factor, sigma32, reveals a multifaceted cellular response to heat stress.
566 Genes Dev. 2006;20: 1776–1789. doi:10.1101/gad.1428206

567 14. John J, Jabbar J, Badjatia N, Rossi MJ, Lai WKM, Pugh BF. Genome-wide promoter assembly in E.
568 coli measured at single-base resolution. Genome Res. 2022;32: 878–892.
569 doi:10.1101/gr.276544.121

570 15. Nielsen HJ, Ottesen JR, Youngren B, Austin SJ, Hansen FG. The Escherichia coli chromosome is
571 organized with the left and right chromosome arms in separate cell halves. Mol Microbiol.
572 2006;62: 331–338. doi:10.1111/j.1365-2958.2006.05346.x

573 16. Tosa T, Pizer LI. Biochemical bases for the antimetabolite action of L-serine hydroxamate. J
574 Bacteriol. 1971;106: 972–982. doi:10.1128/jb.106.3.972-982.1971

575 17. Gourse RL, Chen AY, Gopalkrishnan S, Sanchez-Vazquez P, Myers A, Ross W. Transcriptional
576 Responses to ppGpp and DksA. Annu Rev Microbiol. 2018;72: 163–184. doi:10.1146/annurev-
577 micro-090817-062444

578 18. Zhang Y, Gross CA. Cold Shock Response in Bacteria. Annu Rev Genet. 2021;55: 377–400.
579 doi:10.1146/annurev-genet-071819-031654

580 19. Cao H, Wei D, Yang Y, Shang Y, Li G, Zhou Y, et al. Systems-level understanding of ethanol-
581 induced stresses and adaptation in E. coli. Sci Rep. 2017;7: 44150. doi:10.1038/srep44150

582 20. Macvanin M, Edgar R, Cui F, Trostel A, Zhurkin V, Adhya S. Noncoding rnas Binding to the
583 Nucleoid Protein HU in Escherichia coli. J Bacteriol. 2012;194: 6046–6055. doi:10.1128/JB.00961-
584 12

585 21. Ladouceur AM, Parmar BS, Biedzinski S, Wall J, Tope SG, Cohn D, et al. Clusters of bacterial RNA
586 polymerase are biomolecular condensates that assemble through liquid-liquid phase separation.
587 Proc Natl Acad Sci U S A. 2020;117: 18540–18549. doi:10.1073/pnas.2005019117

588 22. Cui L, Vigouroux A, Rousset F, Varet H, Khanna V, Bikard D. A CRISPRi screen in E. coli reveals
589 sequence-specific toxicity of dCas9. Nat Commun. 2018;9: 1912. doi:10.1038/s41467-018-04209-
590 5

591 23. Lee C, Cox RM, Papoulas O, Horani A, Drew K, Devitt CC, et al. Functional partitioning of a liquid-
592 like organelle during assembly of axonemal dyneins. Carter AP, Akhmanova A, Stearns T, Kikkawa
593 M, editors. Elife. 2020;9: e58662. doi:10.7554/eLife.58662

594 24. Yang D, Ye X, Lorimer GH. Symmetric GroEL: GroES2 complexes are the protein-folding functional
595 form of the chaperonin nanomachine. Proc Natl Acad Sci U S A. 2013;110.
596 doi:10.1073/pnas.1318862110

597 25. Fayet O, Ziegelhoffer T, Georgopoulos C. The groES and groEL heat shock gene products of
598 Escherichia coli are essential for bacterial growth at all temperatures. J Bacteriol. 1989;171:
599 1379–1385. doi:10.1128/jb.171.3.1379-1385.1989

600 26. Cowing DW, Bardwellt JCA, Craigt EA, Woolfordt C, Hendrixt RW, Gross CA. Consensus sequence
601 for Escherichia coli heat shock gene promoters (transcription initiation/ar factors/dnaK regulon).
602 Proc Nati Acad Sci USA. 1985. Available: https://www.pnas.org

603 27. Guisbert E, Herman C, Lu CZ, Gross CA. A chaperone network controls the heat shock response in
604 E. coli. Genes Dev. 2004;18: 2812–2821. doi:10.1101/gad.1219204

605 28. Lim B, Miyazaki R, Neher S, Siegele DA, Ito K, Walter P, et al. Heat shock transcription factor σ32
606 co-opts the signal recognition particle to regulate protein homeostasis in E. coli. PLoS Biol.
607 2013;11: e1001735. doi:10.1371/journal.pbio.1001735

608 29. Yura T, Guisbert E, Poritz M, Lu CZ, Campbell E, Gross CA. Analysis of \&\#x3c3;^{32} mutants
609 defective in chaperone-mediated feedback control reveals unexpected complexity of the heat
610 shock response. Proceedings of the National Academy of Sciences. 2007;104: 17638–17643.
611 doi:10.1073/pnas.0708819104

612 30. Maeda H, Fujita N, Ishihama A. Competition among seven Escherichia coli σ subunits: relative
613 binding affinities to the core RNA polymerase. Nucleic Acids Res. 2000;28: 3497–3503.
614 doi:10.1093/nar/28.18.3497

615 31. Ishihama A. Functional Modulation of Escherichia Coli RNA Polymerase. Annu Rev Microbiol.
616 2000;54: 499–518. doi:10.1146/annurev.micro.54.1.499

617 32. Joo DM, Nolte A, Calendar R, Zhou YN, Jin DJ. Multiple regions on the Escherichia coli heat shock
618 transcription factor sigma32 determine core RNA polymerase binding specificity. J Bacteriol.
619 1998;180: 1095–1102. doi:10.1128/JB.180.5.1095-1102.1998

620 33. Harshey RM. Transposable Phage Mu. 2014. doi:10.1128/microbiolspec

621 34. Belton J-M, McCord RP, Gibcus JH, Naumova N, Zhan Y, Dekker J. Hi-C: a comprehensive
622 technique to capture the conformation of genomes. Methods. 2012;58: 268–276.
623 doi:10.1016/j.ymeth.2012.05.001

624 35. Mcstay B. The p-Arms of Human Acrocentric Chromosomes Play by a Different Set of Rules.
625 Annual Review of Genomics and Human Genetics Annu Rev Genom Hum Genet 2023. 2024;24:
626 48. doi:10.1146/annurev-genom-101122

627 36. Sochorová J, Gálvez F, Matyášek R, Garcia S, Kovařík A. Analyses of the updated “animal rdna loci
628 database” with an emphasis on its new features. Int J Mol Sci. 2021;22.
629 doi:10.3390/ijms222111403

630 37. Tsuneaki A, Ciarán C, Justina V, Dmitry Z, Binghua S, Michaal A-O, et al. Construction and Initial
631 Characterization of Escherichia coli Strains with Few or No Intact Chromosomal rRNA Operons. J
632 Bacteriol. 1999;181: 3803–3809. doi:10.1128/jb.181.12.3803-3809.1999

633 38. Campbell EA, Korzheva N, Mustaev A, Murakami K, Nair S, Goldfarb A, et al. Structural
634 Mechanism for Rifampicin Inhibition of Bacterial RNA. Cell. 2001.

635 39. Dash S, Lamb MC, Lange JJ, McKinney MC, Tsuchiya D, Guo F, et al. rRNA transcription is integral
636 to phase separation and maintenance of nucleolar structure. PLoS Genet. 2023;19.
637 doi:10.1371/journal.pgen.1010854

638 40. Enz S, Braun V, Crosa JH. Transcription of the region encoding the ferric dicitrate-transport
639 system in Escherichia coli: similarity between promoters for fecA and for extracytoplasmic
640 function sigma factors. Gene. 1995;163: 13–18. doi:10.1016/0378-1119(95)00380-o

641 41. Enz S, Mahren S, Stroeher UH, Braun V. Surface signaling in ferric citrate transport gene
642 induction: interaction of the FecA, FecR, and FecI regulatory proteins. J Bacteriol. 2000;182: 637–
643 646. doi:10.1128/JB.182.3.637-646.2000

644 42. Ferguson AD, Chakraborty R, Smith BS, Esser L, van der Helm D, Deisenhofer J. Structural Basis of
645 Gating by the Outer Membrane Transporter FecA. Science (1979). 2002;295: 1715–1719.
646 doi:10.1126/science.1067313

647 43. Susanne M, Volkmar B. The FecI Extracytoplasmic-Function Sigma Factor of Escherichia coli
648 Interacts with the β′ Subunit of RNA Polymerase. J Bacteriol. 2003;185: 1796–1802.
649 doi:10.1128/jb.185.6.1796-1802.2003

650 44. Erickson JW, Gross CA. Identification of the sigma E subunit of Escherichia coli RNA polymerase:
651 a second alternate sigma factor involved in high-temperature gene expression. Genes Dev.
652 1989;3: 1462–1471. doi:10.1101/gad.3.9.1462

653 45. Missiakas D, Raina S. The extracytoplasmic function sigma factors: role and regulation. Mol
654 Microbiol. 1998;28: 1059–1066. doi:10.1046/j.1365-2958.1998.00865.x

655 46. Missiakas D, Mayer MP, Lemaire M, Georgopoulos C, Raina S. Modulation of the Escherichia
656 coliσE (RpoE) heat-shock transcription-factor activity by the RseA, RseB and RseC proteins. Mol
657 Microbiol. 1997;24: 355–371. doi:https://doi.org/10.1046/j.1365-2958.1997.3601713.x

658 47. Campbell EA, Tupy JL, Gruber TM, Wang S, Sharp MM, Gross CA, et al. Crystal Structure of
659 Escherichia coli σE with the Cytoplasmic Domain of Its Anti-σ RseA. Mol Cell. 2003;11: 1067–
660 1078. doi:https://doi.org/10.1016/S1097-2765(03)00148-5

661 48. Kanehara K, Ito K, Akiyama Y. YaeL proteolysis of RseA is controlled by the PDZ domain of YaeL
662 and a Gln-rich region of RseA. EMBO J. 2003;22: 6389–6398.
663 doi:https://doi.org/10.1093/emboj/cdg602

664 49. Ades SE, Connolly LE, Alba BM, Gross CA. The Escherichia coli sigma(E)-dependent
665 extracytoplasmic stress response is controlled by the regulated proteolysis of an anti-sigma
666 factor. Genes Dev. 1999;13: 2449–2461. doi:10.1101/gad.13.18.2449

667 50. Ishihama A. Subunit of assembly of Escherichia coli RNA polymerase. Adv Biophys. 1981;14: 1–35.

668 51. Mathew R, Chatterji D. The evolving story of the omega subunit of bacterial RNA polymerase.
669 Trends in Microbiology. 2006. pp. 450–455. doi:10.1016/j.tim.2006.08.002

670 52. Ross W, Gosink KK, Salomon J, Igarashi K, Zou C, Ishihama A, et al. A Third Recognition Element in
671 Bacterial Promoters: DNA Binding by the α Subunit of RNA Polymerase. Science (1979). 1993;262:
672 1407–1413. doi:10.1126/science.8248780

673 53. Ziemienowicz A, Skowyra D, Zeilstra-Ryallsqli J, Fayet O, Georgopoulos C, Zylicz MY. The Journal
674 of Biological Chemistry. Both the Escherichia coli Chaperone Systems, GroEL/GroES and
675 DnaKIDnaJIGrpE, Can Reactivate Heat-treated RNA Polymerase. 1993.

676 54. Cabrera JE, Jin DJ. The distribution of RNA polymerase in Escherichia coli is dynamic and
677 sensitive to environmental cues. Mol Microbiol. 2003;50: 1493–1505. doi:10.1046/j.1365-
678 2958.2003.03805.x

679 55. Stracy M, Lesterlin C, Garza de Leon F, Uphoff S, Zawadzki P, Kapanidis AN. Live-cell
680 superresolution microscopy reveals the organization of RNA polymerase in the bacterial nucleoid.
681 Proc Natl Acad Sci U S A. 2015/07/29. 2015;112: E4390–E4399. doi:10.1073/pnas.1507592112

682 56. Jin DJ, Cagliero C, Zhou YN. Growth rate regulation in Escherichia coli. FEMS Microbiol Rev.
683 2012;36: 269–287. doi:10.1111/j.1574-6976.2011.00279.x

684 57. Weng X, Bohrer CH, Bettridge K, Lagda AC, Cagliero C, Jin DJ, et al. Spatial organization of RNA
685 polymerase and its relationship with transcription in Escherichia coli. Proceedings of the National
686 Academy of Sciences. 2019;116: 20115–20123. doi:10.1073/pnas.1903968116

687 58. Gibson DG, Young L, Chuang R-Y, Venter JC, Hutchison CA, Smith HO. Enzymatic assembly of DNA
688 molecules up to several hundred kilobases. Nat Methods. 2009;6: 343–345.
689 doi:10.1038/nmeth.1318

690 59. Datsenko KA, Wanner BL. One-step inactivation of chromosomal genes in *Escherichia coli* K-12
691 using PCR products. Proceedings of the National Academy of Sciences. 2000;97: 6640–6645.
692 doi:10.1073/pnas.120163297

693

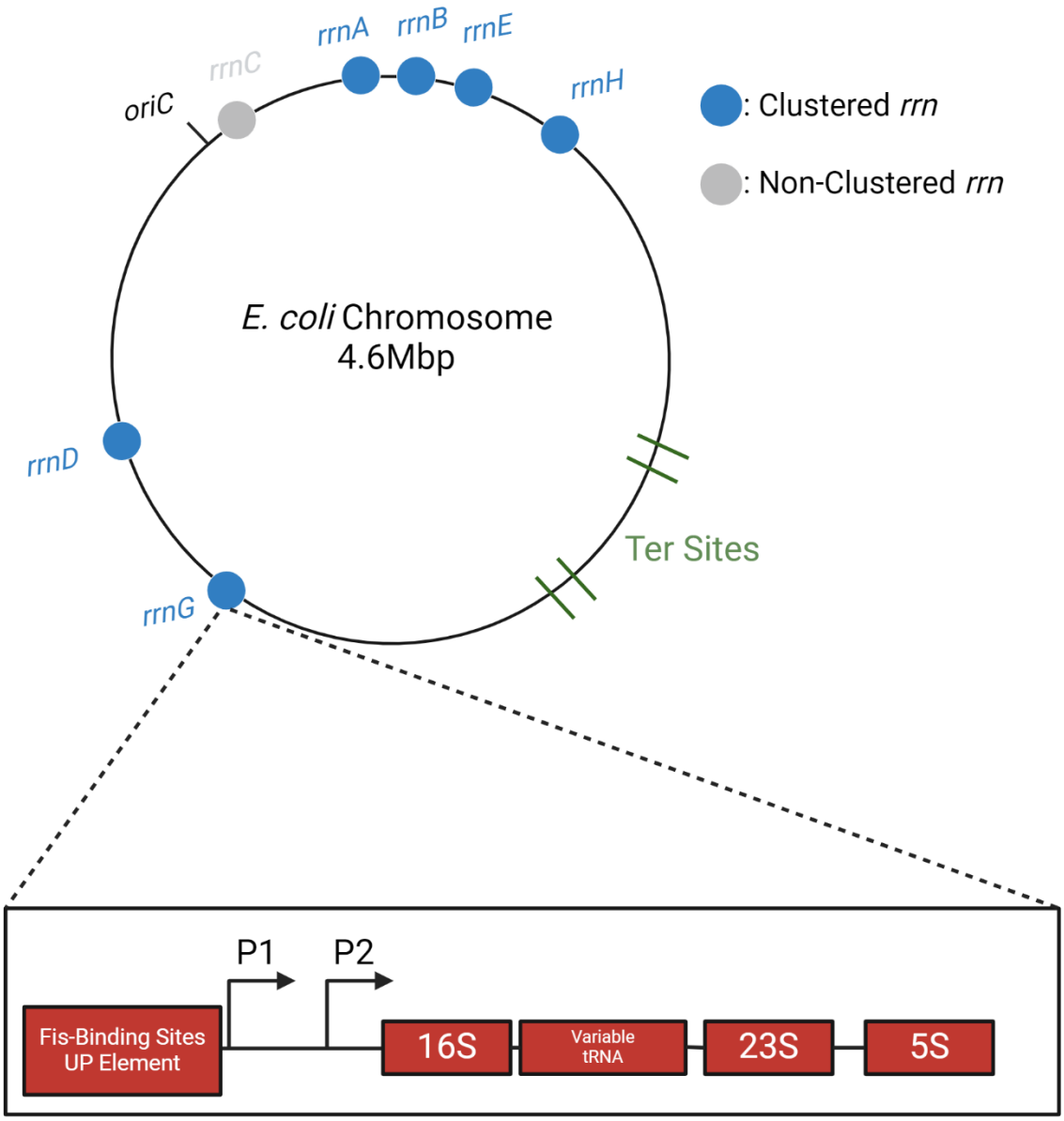

Fig. 1*: Distribution of rrn operons on the E. coli genome*. On the circular *E. coli* chromosome, replication originates at *oriC*, with two bidirectional replication forks traversing each arm (replicore), terminating within the Ter region. Locations of the *rrn* operons shown to cluster by two different methodologies (see text) are indicated by blue-filled circles. Organization of a typical *rrn* operon is shown for *rrnG*; P1 and P2 promoters are indicated by arrows.

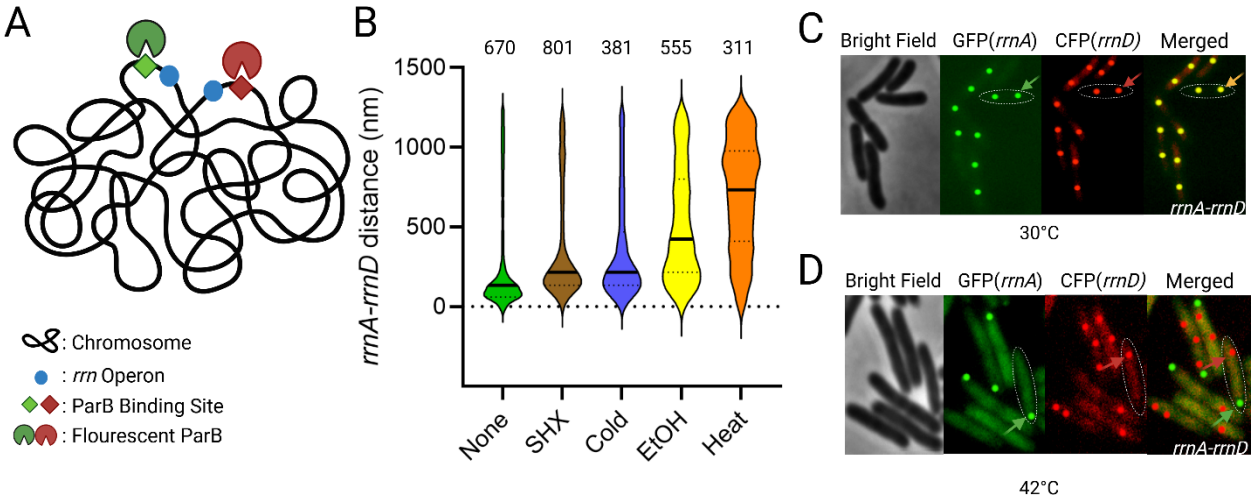

Fig. 2: Distance between *rrnA* and *rrnD* operons under various stress conditions. (A) Scheme for *rrn* operon tagging. Two different *par* sites (*parS*T1 and *parS*P1) were placed upstream of *rrnA* and *rrnD*, respectively, in the parent strain MG1655. These sites were visualized by co-expression of their cognate fluorescent ParB proteins (pMT1 GFP-ParB and P1 CFP-ParB). (B) Violin plots of the distance between *rrnA* and *rrnD* under indicated stress conditions (see Methods for details). The numbers on the top refer to *rrn* pairs observed for one of three biological replicates. The solid line indicates the median distance, and the top and bottom dashed lines indicate the 3rd and 1st quartile, respectively. We note that due to the large number of foci observed, a small change in the median distance is considered statistically significant ($p<0.001$) under Mann-Whitney test. We arbitrarily considered a 2-fold change of median distance to be significant. (C) Images used to generate data in (B). Representative image of *rrnA*-*rrnD* clustering without added stress. GFP and CFP were false-colored and enhanced for better visualization. One cell is outlined, with an arrow pointing to a merged GFP/CFP focus. The foci are edited in post-processing as a perfect circle to provide better contrast and visualization. Most cells appear to contain 2 copies of the *rrn* operons, indicating that this region of the chromosome is replicated. (D) Representative image of *rrnA*-*rrnD* de-clustering with heat stress. Colored arrows indicate focus from either GFP-field (green) or CFP (red). We note that the number of *rrnA*-GFP foci is reduced to 1 focus per cell.

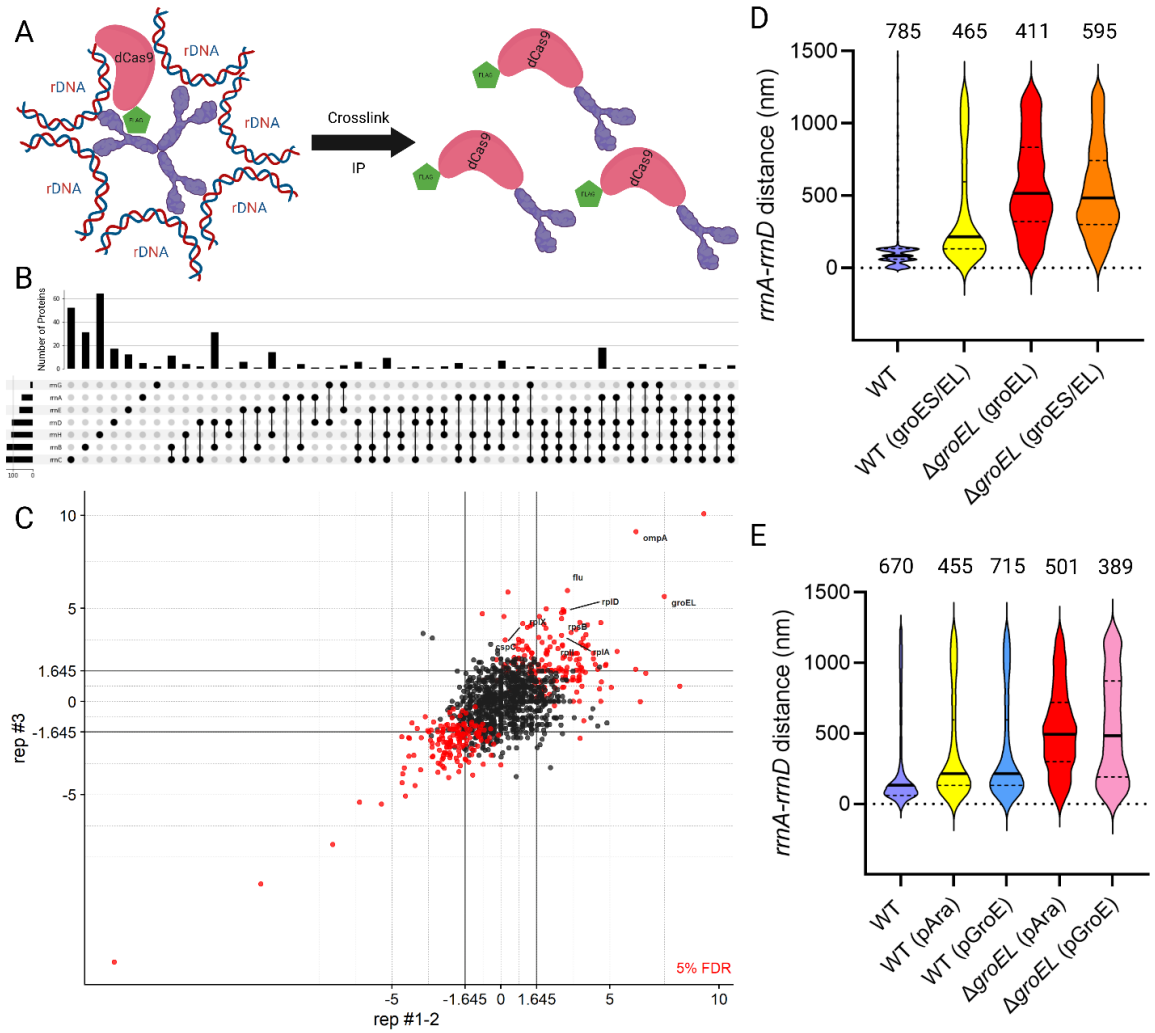

Fig. 3: Deregulation of GroEL disrupts *rrnA-rrnD* clustering. (A) Scheme for pulldown of proteins in the vicinity of all *rrn* loci. dCas9-FLAG (pink/green) was directed upstream of all 7 *rrn* loci by expressing sgRNA specific for each target. Formaldehyde was used to crosslink dCas9 to putative bridging factor(s) (purple). The dCas9-linked 'complex' was then immunoprecipitated and subjected to mass spectrometry (MS). (B) Aggregated MS results of significantly enriched proteins from dCas9 pulldown. The bar graph shows the number of proteins identified for each combination. The black ball indicates the pulldown of the sgRNA of interest, and the black line connecting them indicates co-occurrence of the proteins in the indicated sgRNA pulldowns. (C) Significantly enriched proteins in pulldown with gRNA targeting *yeiP* (*rrnC*). Each protein is identified by a circle. Each axis represents the z-score of each protein in separate experiments. Lines from the axes indicate the cut-off for enrichment. Red circles and black circles indicate proteins that fall above and below the False Discovery Rate (FDR) (5%), respectively. Proteins significantly enriched are in the top-right square (z score>2.5) with the protein name in red. See Fig. S4 for data obtained for the remaining gRNAs. (D) Distance between *rrnA-D* operons in WT and Δ*groEL* strains expressing either both *groES/groEL* or *groEL* alone from pAraBAD plasmid. Other descriptions as in Fig. 2. (E) Distance between *rrnA-D* in WT and Δ*groEL* strains expressing *groES/groEL* from either pAra or the native *groE* promoter.

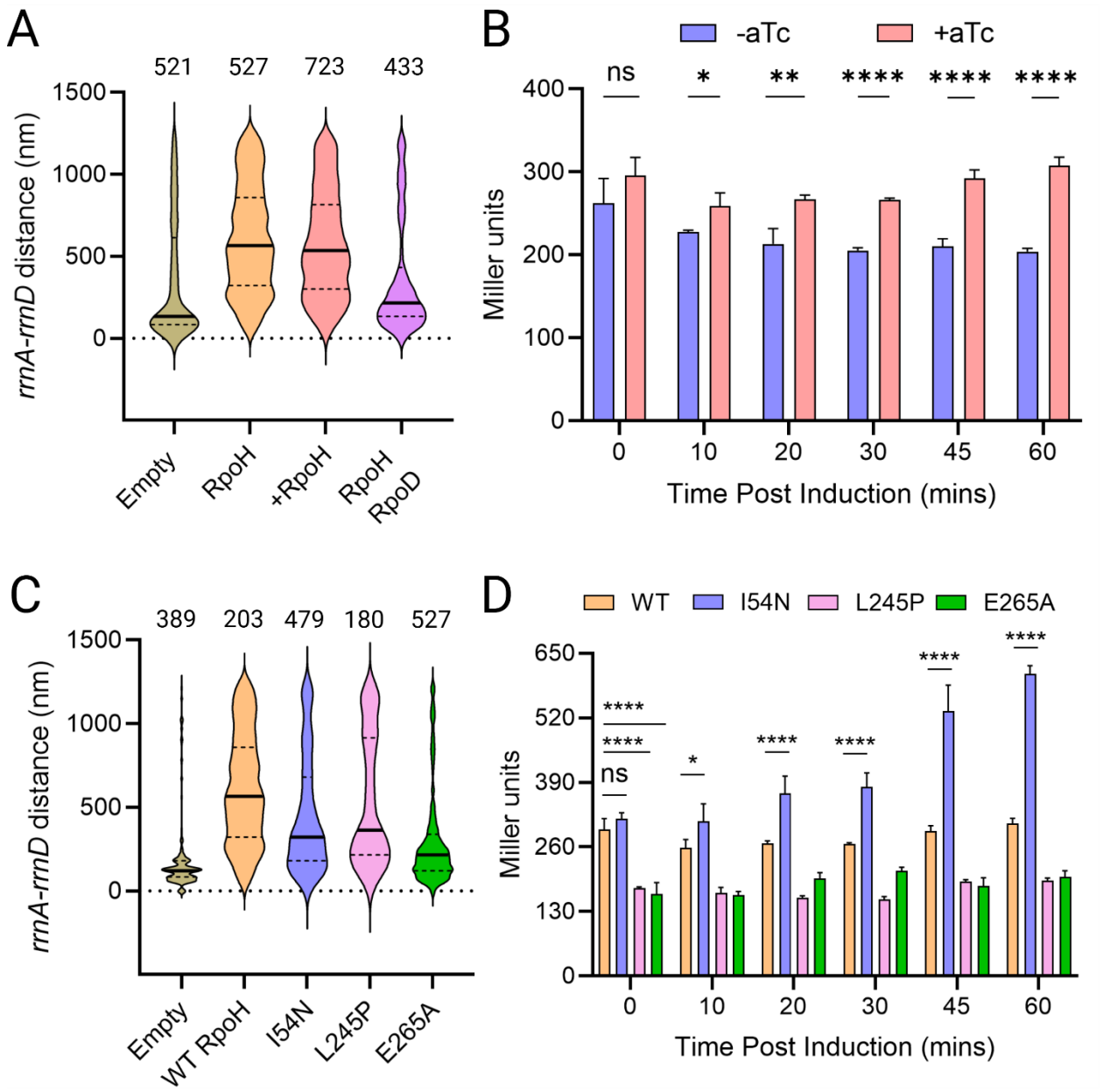

Figure 4: **σ^H promotes de-clustering of *rrnA-rrnD* independent of its transcriptional activity**
(A) Distance between *rrnA-D* with ectopic expression of *rpoH* from pTc. Induction was carried out for one hour prior to microscopy. In the 4th plot from left, RpoD is cloned downstream of TetR, from a constitutively expressed promoter, divergent from pTc. All other descriptions as in Fig. 2. (B) Transcriptional activity of ectopically expressed *rpoH*. Miller assay was carried out as described in Methods. Student t's test was performed pairwise to determine statistical significance (two tailed, ns: not statistically significant, *: $p<0.05$, **: $p< 0.01$, ****: $p< 0.0001$). (C) Distance between *rrnA-D* with ectopic expression of indicated *rpoH* mutants, compared to empty vector control. (D) Transcriptional activity of ectopically expressed *rpoH* mutants, as described in B.

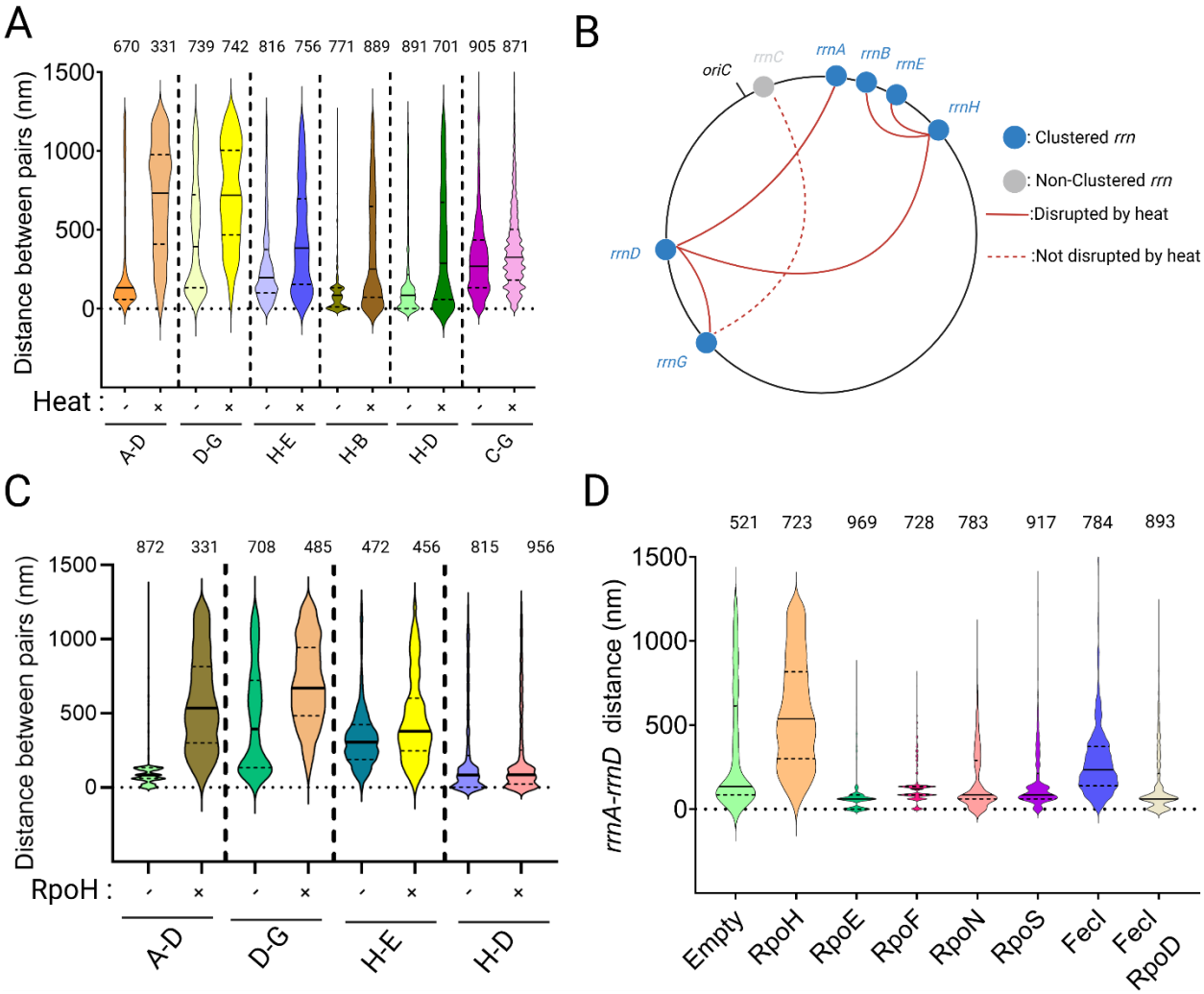

Figure 5: Disruption of *rrn* clustering by heat stress and by FecI. (A) Effect of heat stress on clustering of *rrn* pairs. Other descriptions as in Fig. 2. (B) Response to heat stress of tested *rrn* pairs. Each of the 7 *rrn* operons was visited at least once. (C) Response to *rpoH* induction of tested *rrn* pairs. (D) Effect of ectopic expression of five σ factors on clustering *rrnA-D*, all placed under control of pTc with the same RBS. +/- symbols are self-explanatory.

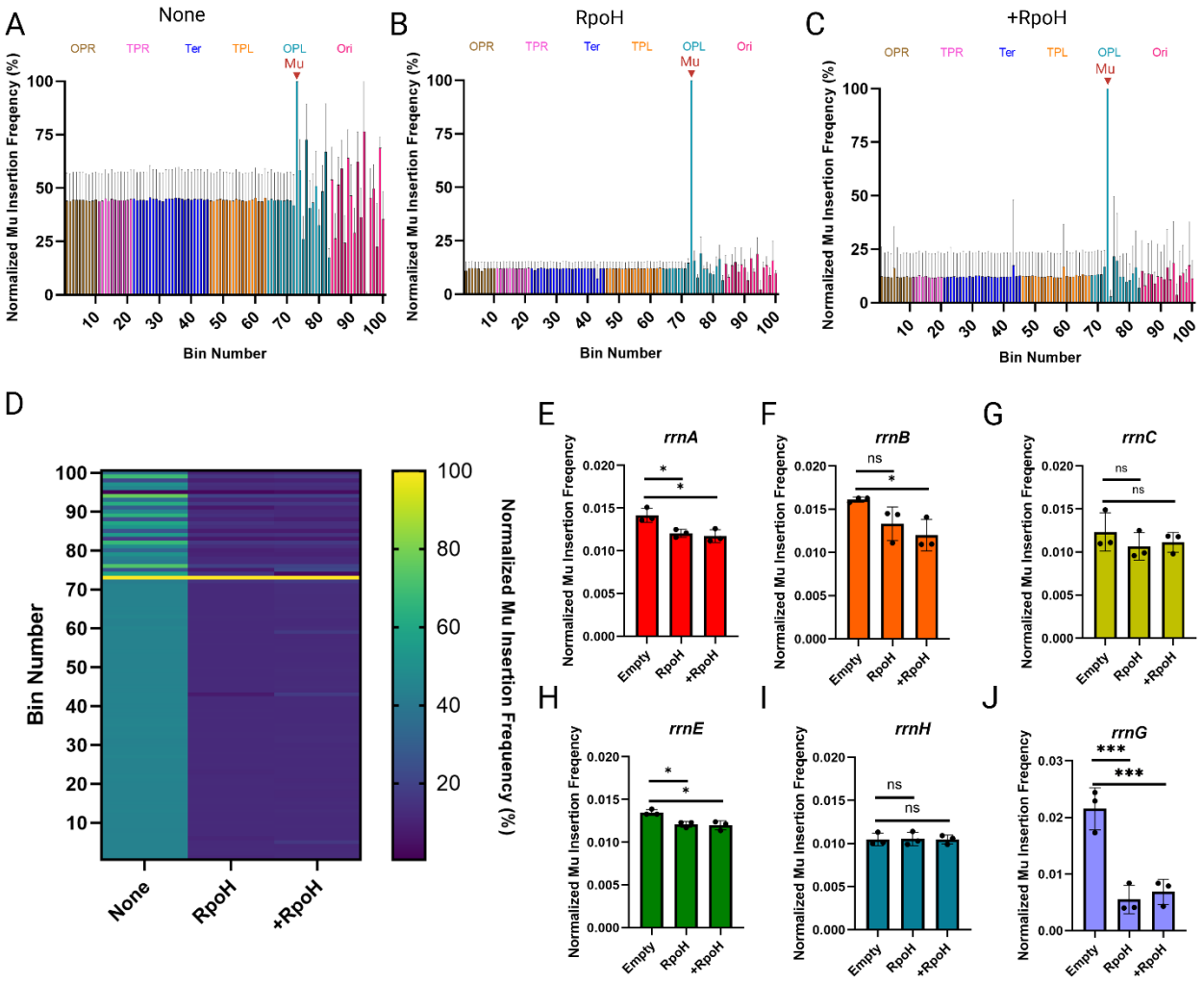

Figure 6: Expression of *rpoH* promotes local chromosomal contacts. (A) Frequency of transposition of Mu located in the vicinity of *rrnD* (Bin 72) after one round of transposition. The number of insertions has been normalized to the read depth of each bin. The initial Mu position is indicated by a red triangle. The *E. coli* genome was partitioned into 100 equally sized bins, so each bin is ~46 kb. Starting Bin #s and chromosomal regions are indicated on top. Each vertical bar represents the average normalized transposition frequency of 3 biological replicates at the indicated bin, expressed as a percentage (with the highest transposition frequency being set to 100%). Grey error bars are the standard deviation. Color bars indicate regions of the *E. coli* chromosome annotated up top. (B) Same as (A) but with the *rpoH* overexpression vector. (C) Same as (B) but with induction of *rpoH* expression. (D). Heat map of the data from A through C. (E-J). Transposition frequency from *mlaF* (*rrnD*) into the indicated *rrn* operon-containing bin under conditions described in A through C. The individual data points and associated standard deviation are shown. Statistical significance was determined with Student t's test (two-tailed), *: $p<0.05$. ns: not statistically significant.

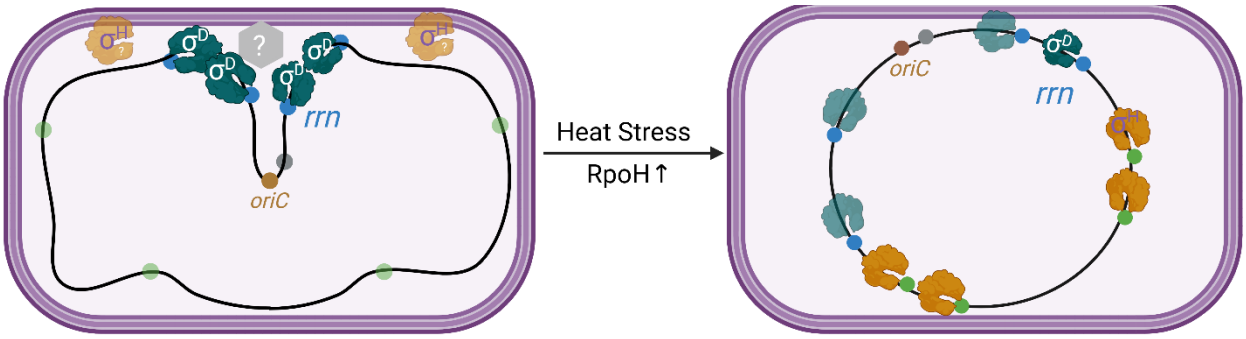

Figure 7: Model for *rrn* clustering mediated by σ^D. Left: Clustering of *rrn* operons is mediated by σ^D at the membrane either through σ^D directly or through other unknown factor(s) (grey hexagon). Upon heat stress or elevated σ^H levels, RNAP complexes (dark green) bound to σ^D transcribing the *rrn* operons (blue circles) are displaced through competition with σ^H, which is typically localized to the inner membrane and degraded. RNAP-core complexed with σ^H (orange) transcribes genes in σ^H regulon (green circles), lowering the total amount of RNAP transcribing *rrn* operons at the membrane, resulting in their de-clustering.